



ISSN NO. 2320-5407

Journal Homepage: - www.journalijar.com

INTERNATIONAL JOURNAL OF ADVANCED RESEARCH (IJAR)

Article DOI: 10.21474/IJAR01/2140
DOI URL: <http://dx.doi.org/10.21474/IJAR01/2140>



INTERNATIONAL JOURNAL OF
ADVANCED RESEARCH (IJAR)
ISSN 2320-5407
Journal homepage: <http://www.journalijar.com>
Journal DOI: 10.21474/IJAR01

RESEARCH ARTICLE

STRUCTURAL, DIELECTRIC AND A.C. CONDUCTIVITY STUDIES OF $BaCe_{0.65}Zr_{0.2}Y_{0.15}O_{3-\delta}$ SOLID OXIDE FUEL CELL ELECTROLYTE BY CITRATE EDTA COMPLEXING SOL-GEL PROCESS.

J. Madhuri Sailaja¹, N. Murali², K. Vijay Babu² and V. Veeraiah¹.

1. Department of Physics, Andhra University, Vishakhapatnam, Andhra Pradesh, India.
2. Advanced Analytical Laboratory, DST-PURSE Programme, Andhra University.

Manuscript Info

Manuscript History

Received: 25 September 2016
Final Accepted: 27 October 2016
Published: November 2016

Key words:-

Perovskite, $BaCe_{0.65}Zr_{0.2}Y_{0.15}O_3$, Sol-Gel synthesis, Fuel Cells, dielectric properties

Abstract

This paper reports on the effect of Zirconium doping on $BaCe_{0.85}Y_{0.15}O_{3-\delta}$ electrolyte prepared using the citrate-EDTA complexing modified sol-gel process at calcinations temperature $T=1000^\circ\text{C}$.

The phase formation, Thermal analysis, Morphology, Stability and Conductivity measurements were performed on the sintered powders through Thermogravimetric analysis (TGDTA), Xray diffraction (XRD), Scanning electron microscope (SEM), EDAX, FTIR, RAMAN and LCR measurements. The crystallite size of the ceramic powders calculated from Scherrer equation is 26.49nm and microstructure of the sintered powder revealed that the average grain size is in the range of 2-3 μm . Dense ceramic materials were obtained at 1300°C and the relative density is 90% of the theoretical density. The ionic conductivity of the pellet is investigated from room temperature to 500°C and is found to exhibit highest conductivity of $2.2 \times 10^{-3} \text{S/cm}$ and $2.76 \times 10^{-3} \text{S/cm}$ at 500°C in dry air and wet air atmosphere with 3% relative humidity. Frequency dependence on the dielectric constant has been investigated at various temperatures which clarified that larger value of ϵ is due to superposition of both electrolyte –electrode interfacial and space charge polarization originated from dopant-vacancies created. The conductivity increased as temperature increases with activation energy in the range 0.5eV and hence this composition is worth being an electrolyte.

Copy Right, IJAR, 2016., All rights reserved.

Introduction:-

As the consumption of energy across the globe is continuously increasing and people's consciousness towards protection of environment is widely sprouting out, developing and employing clean energy source have been paid great attention worldwide. Intermediate solid oxide fuel cells (IT-SOFCs) have provoked special interest as future renewable energy option due to their high efficiency and low environmental pollution [1-4]. These fuel cells consists of either oxygen ion or proton conducting electrolyte material which is free from dilution of fuel with water as by products. In particular perovskite oxides based on $BaCeO_3$ or $SrCeO_3$ doped with some trivalent cations exhibit high protonic conductivity at temperatures $>300^\circ\text{C}$ when exposed to wet atmospheres containing hydrogen [5, 6]. Several

Corresponding Author:- J. Madhuri Sailaja.

Address:- Department of Physics, Andhra University, Vishakhapatnam, Andhra Pradesh, India.

researches have successfully synthesized BCY electrolyte but one drawback of these materials is their instability to CO₂ atmospheres which hinders practical limitations [7-11].

In contrast, the chemical stability of doped barium Zirconates is far greater which may be due to its high covalence of Zr-O bond but exhibited low conductivity [5, 9, and 11]. Therefore in order to have proton conducting electrolytes with enhanced proton conductivity and good chemical stability, the use of cerate-zirconate solid solutions has been experimented and recent reports proved the same. Various methods of preparations are reported in literature using solid state reaction method and sol-gel method using ethylene glycol [9, 10, 12, and 13]. For e.g. Zuo et.al [14] reported that BaCe_{0.7}Zr_{0.1}Y_{0.2}O_{3-δ} (BZCY) electrolyte displayed both satisfactory conductivity and sufficient chemical stability over a wide range of conditions relevant to fuel cell applications. Thus the present work is focused on modified Sol-Gel method and the influence of preparation technique on structure and conductivity at low sintering temperatures.

Experimental:-

Powder preparation:-

The citrate-EDTA complexing sol-gel synthesis method is used for preparing BaCe_{0.65}Zr_{0.2}Y_{0.15}O_{3-δ} oxide. The starting materials for this process are commercial Ba (NO₃)₂, ZrO(NO₃)₂·2H₂O, Ce (NO₃)₃·6H₂O, Y(NO₃)₃·6H₂O (Sigma Aldrich, 99.9%). Both citric acid and EDTA are slowly added to the precursor solution as chelating agents. The EDTA molar ratio and citric acid to the total metal cations content was set at 1:2:1. The pH value of the solution was adjusted to be around 6 using NH₄OH. The mixed solutions were heated under stirring until obtaining viscous gels at T=100°C. Additional heating at T=250°C evaporates residual water & any organic material present until these gels get transformed into black powders. The synthesized powder is then calcined at T=1000°C for a period of 12h at a heating rate of 5°C/min which resulted in fine yellow powders. To obtain dense sample, the calcined powder is uniaxially pressed into cylindrical pellet under 5 ton pressures for 300sec and then sintered in an air atmosphere. Sintering was carried out at T=1300°C for 5h at a heating rate of 5°C/min. Small amount of powder of same composition is sprinkled on the both sides of the pellet while sintering to avoid Ba deficiency due to evaporation. Silver paste (Alfa Aesar) is applied on both the sides of the pellet for providing electrical contact and electrical connections by ultrafine pure (99.9%) silver wires (Alfer Aesar) and heated at a temperature of 350°C for 30mts prior to impedance measurements. For the purpose of comparison, the composition BaCe_{0.85}Y_{0.15}O₃ synthesized using the same method of preparation reported elsewhere is quoted [30].

Characterization:-

Thermo gravimetric analysis (TGA) are performed to the dried powder (T= 250°C) by a TA instrument model SDTQ 600. The phase identification of the sintered oxides is performed with a powder Diffractometer (PANalytical X-pert Pro) filled with Ni filtered Cu Ka radiation and the diffraction angle from 10° to 90° with a step of 0.01°/min. The unit cell parameters are obtained by unit cell software from the 2θ and (h k l) values. Morphologies of the sintered pellet is scrutinized using scanning electron microscope JEOL model JSM-6610 LV along with an energy dispersion spectrometer (EDS) Inca Penta FETX3.JPG 8900 Spectrometer to find out the percentage of elements in the sample. A FTIR spectrometer instrument (SHIMADZU IR Prestige-21, Singapore) is used to record the FTIR spectra of BaCe_{0.65}Zr_{0.2}Y_{0.15}O₃ powder in the range of 3,000-400cm⁻¹ and in turn investigate the formation of complex structure, carbonates and oxides. The theoretical density of the sample is calculated with the obtained XRD. LCR measurements from 30-500°C in air atmosphere and wet air with 3% relative humidity were performed with Wayneker P6500 model in the frequency range from 20Hz to 1 MHz.

Results and Discussion:-

Thermogravimetry / Differential Thermal Analysis:-

To investigate the reaction of the perovskite phase structure formation, simultaneous TG-DTA curves of the sample measured from 30-1200°C are presented in Fig 1. In general thermal stability of nitrates less when compared to carbonates and hence is easy to decompose.

The formation of multi component perovskite materials involves the rearrangement of cations and oxygen ions during the synthesis. As solid state reaction method involves high calcinations temperatures which leads to barium evaporation, Sol-Gel technique has the ease of homogenous mixing of cations at the atomic level in the precursor stage thus facilitating the formation of a stable phase compound at low temperatures. From Fig.1 it can be seen that three regions are obtained in TG-DTA of the powder. The first stage of the TG profile upto 150° may be attributed

to the evaporation of residual water, free nitric acid decomposition and some nitric acid removal. The weight loss in the range 150-300°C may probably be due to the thermal decomposition of the citrate complex and burning of citrate chains corresponding to an exothermic peak at 45°C. The additional weight loss along with exothermal peaks in DTA discloses that the decomposition of gel takes place in two steps. The weight loss from 300°C to 500°C is found to be 17% followed by a small exothermic peak at 405°C is due to combustion of the metal nitrates. The drastic weight loss seen from 500-630°C (37%) and the exothermic peak at T=569°C is due to co-oxidation. A very small weight loss is recorded at T >1000°C which is due to barium carbonate thermal decomposition and the formation of powder with the release of CO₂ [15, 16]. This is consistent with the XRD results from the Fig.2 that BaCe_{0.65}Zr_{0.2}Y_{0.15}O_{3-δ} phase only forms upon calcining at 1000°C and above. There is no apparent weight change is reported when the temperature is higher than 1000°C, indicating complete phase formation of the compound which is evident from TG-DTA measurements.

X-ray diffraction (XRD) analysis:-

The phase composition of BaCe_{0.65}Zr_{0.2}Y_{0.15}O_{3-δ} powder has been identified by X-ray diffraction (XRD) analysis. The experimental diffraction pattern is collected at room temperature by step scanning at 0.01°/min over the range 10° ≤ 2θ ≤ 90°. As shown in Fig.2a sintered oxides are predominantly the perovskite dominant structure with seven major diffraction peaks (002), (022), (231), (422), (024), (440) and (613) planes (JCPDS Card no. 22-0074). The XRD patterns of powders calcined at T=1000°C for 12h showed a single orthorhombic phase with pnma space group according to Knight et al. [17-21]. The cell parameters of both calcined and sintered were determined by least-square refinements and the calculated lattice parameters are found to be a=8.67145, b=6.148, c=6.236 and cell volume is 332.490(Å)³ with a relative density of 90% which are consistent with that available in the literature [31]. The lattice volumes of both the samples reflected the same trend except an increase in the lattice volume which may be due to increase in the thermal reduction of Ce⁴⁺ to Ce³⁺ [22]. It was reported that phase formation in BaCeO₃ obtained from solid state synthesis requires calcinations at 1100°C or 1200°C for 10h or more. Such high temperatures may result in grain growth which causes decrease in surface area of the powder and sintered density. In the present preparation method, 1000°C is sufficient to form a single phase material by adjusting the pH value to 6 which liberates more protons from citric acid that helps to chelate Ba ions and enhance phase formation.

Close examination of the XRD data extrapolate that as zirconium is doped in the B sites the diffraction peak shifted to higher angles and decrease of the lattice parameters along with lattice volume is observed than BaCe_{0.85}Y_{0.15}O₃ (339.4 Å³) [30], which suggests a plane distance reduction (according to Bragg's law). This can be well explained by the fact that Zr⁴⁺ (0.84Å) has a smaller ionic radius than Ce⁴⁺ (0.97) [22].

The crystallite size of the synthesized sample is calculated using Scherrer's formula and the value decreased from 32nm (BaCe_{0.85}Y_{0.15}O₃) [30] to about 26.49 nm for BaCe_{0.65}Zr_{0.2}Y_{0.15}O₃.

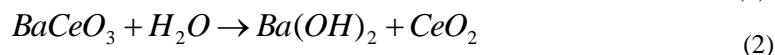
The bulk density of the sintered pellet is measured using Archimedes displacement method. The density of the compound is found to be 90% of the theoretical density. In order to realize the effect of Zr doping on the structural stability, the distortion of cubic lattice was calculated based on the Goldsmith tolerance factor given by the formula

$$t = \frac{r_A + r_O}{\sqrt{2}(r_B + r_O)}$$

Where t is the tolerance factor, r_A is the ionic radius of the A site where Ba²⁺ (1.35Å), r_B is the ionic radius of the B site Ce⁴⁺ (0.87 Å), Zr⁴⁺ (0.72 Å) and Y³⁺ (0.9 Å), r_O is the ionic radius of the oxygen O₂⁻ (1.4 Å). A high value of t, close to unity helps in increasing the stability of the perovskite phase and in the present composition incorporation of Zr increased the tolerance factor from 0.856 (BaCeO₃) to 0.8664 (BaCe_{0.65}Zr_{0.2}Y_{0.15}O_{3-δ}).

Chemical Stability:-

Barium cerate proton conductor is not chemically stable because it can react with CO₂ according to the reaction (1) or with H₂O according to reaction (2)



In order to verify the stability under H₂O containing atmospheres, the sintered pellets are boiled for 2hrs, dried and the XRD patterns are recorded. It has been observed that after exposed to boiling water, the BaCe_{0.85}Y_{0.15}O₃ pellets synthesized through same procedure reported elsewhere showed small BaCO₃ phases as shown in the Fig 2b. Due to reaction with H₂O, BaCO₃ may also form due to interaction with atmospheric CO₂ that converts Ba (OH)₂ into carbonate. On the other these peaks are less intense in BaCe_{0.65}Zr_{0.2}Y_{0.15}O_{3-δ} composition indicating its chemical stability in water.

A neutron Diffraction study shows that, at room temperature and pressure, in the replacement of Zr with Ce, the size of BO₆ octahedral decreases with increase in Zirconium content as Zr acts as a phase stabilizer. Therefore the driving force for the evolution towards a symmetric structure is increased and it becomes more difficult to distort the perovskite structure. This also show that stability in water vapor increases with decreasing ionic radius of the codopant [12, 23].

To check the stability of the material against atmospheric CO₂ small amount is left out in the laboratory for a period of 10 days and the XRD analysis did not show any phase change except for small peaks indicating BaCO₃. These results suggested that when zirconium is doped into barium cerates can definitely improve the chemical stability of BaCe_{0.65}Zr_{0.2}Y_{0.15}O_{3-δ} compounds. It has been reported that the stability of perovskite structures increases with increasing the tolerance factor [12] and this is in agreement with the calculated tolerance factor and experimental lattice parameters of BaCe_{0.65}Zr_{0.2}Y_{0.15}O_{3-δ}. Matsumoto et.al. [34] Investigated chemical stability of BaCeO₃-based proton conductors doping different trivalent cations with thermogravimetry (TG) analysis and found that stability increases with decreasing ionic size of the dopant, which correlate with the present result.

Microstructure:-

The surface morphology of the sintered powder is shown in the Fig 3 depicts a heterogeneous distribution of grains with an average size of 2-3μm. Dense ceramic materials were obtained at T=1300°. The SEM and EDS spectra can be used as a reference to detect possible BaO accumulation at grain boundaries. Present EDX spectra showed that the molar ratio of Ba / (Ce + Zr + Y) is 1.04 at the bulk region which is slightly greater than the ratio of the precursor Ba / (Ce + Zr + Y) = 1:1. The observation of Ba rich phase might be due to powder sprinkled on both sides of the pellet to avoid excess BaO evaporation at high temperatures of sintering.

Fourier transforms infrared spectroscopy (FTIR):-

Fig 6 shows the FTIR spectra obtained with powder prepared by modified Sol-Gel method. FTIR analysis is used to explain in further detail the formation of this carbonate species during heat treatment. The band in the range 500cm⁻¹ originates from the vibrations of Ce-O bonds. The presence of a sharp peak at 856 cm⁻¹ may be due to the =C-H bend and the bands in the region 1049 cm⁻¹ were also assigned to the carbonate peaks (C-O stretch) due to carboxylic group present in the powder burnt to CO₂ during heating and some of the CO₂ molecules are absorbed on the powders. In order to produce the single phase ceramic powders, the decomposition process of the gel should be controlled to suppress the formation of carbonates of constituent species, since those carbonates give possible segregation and in homogeneity in the final oxide powders. The peak localized in the range of 1450-1470cm⁻¹ attributed to the C-H bend and which may be due to the complex formed from a chelating process of chelating agents and metal ions [17, 21]. The transmittance bands around 1638.98 and 1744.5cm⁻¹ may be due to -C=C- and C=O stretch respectively. The peaks near 2800-3000cm⁻¹ are assigned to C-H stretch.

Impedance Spectroscopy:-

The ionic conductivity of ceramic electrolyte depends on physical and chemical properties of the ceramic samples such as composition, ordering ageing effects, grain size and purity. Separation of bulk and grain boundaries conductivity can be accomplished by complex plane analysis. Also the frequency dependent conductivity and dielectric permittivity studies yield important information on the ion transport and relaxation studies of fast ionic conductors.

The impedance spectra measured in dry air from room temperature to 500°C in is shown in the Fig 5. Theoretically the spectra composes of three arcs at low, medium and high frequencies corresponding to the response of electrode, grain boundary and the bulk respectively [23-25] in the Nyquist plots (Z' vs. Z''). The semi circular pattern represents the electrical process taking place that can be expressed in an electrical circuit with a parallel combination of resistive and capacitive elements. In the Nyquist plots of the present work, the high frequency semi circle related to bulk response could not be observed due to the instrumental limitations of the experimental range. Therefore, the

bulk response is ascribed to the high frequency intercept of the medium arc with the real axis which depicted variations of about two to three orders of magnitude with rise in temperature from 30 to 500°C.

The capacitance of any component depends on the relative permeability of the material and on the geometric dimensions of the three frequency regions. The obtained C values of BaCe_{0.65}Zr_{0.2}Y_{0.15}O₃ oxide is found to vary from 10⁻⁹ F for high frequency arc and conserved this value at 10⁻⁷F for low frequency indicating that they corresponds to grain boundary conduction and electrode polarization. The differences observed in C at low temperature may probably be strongly related to the difficulty in the separation of grain and bulk contribution.

Bode plots:-

Nyquist plots are the first choice for EIS measurement but have a drawback e that they do not provide information regarding time or frequency. To avoid this problem Bode plots can be analyzed. The variations of real (Z') and imaginary (Z'') parts of impedance with frequency at different temperatures are shown in the Fig 6. The Z' values decreased sharply with increase in frequency and display characteristic dispersion at low frequencies.

The value of Z'' increased with a rise in frequency followed by a decrease and the peak positions shifted towards higher frequency side along with peak broadening with rising temperatures as shown in Fig 7. The asymmetric broadening of peaks in Z'' vs. frequency entails that there is a spread of relaxation time which indicates a temperature dependence electrical relaxation phenomenon in the material [26]. The peak in the lower frequency region may appear due to the electrode polarization.

Ac conductivity studies:-

The Ac conductivity is calculated from dielectric data using the relation (3)

$$\sigma_{AC} = \omega \epsilon_r \epsilon_0 \tan \sigma \quad (3)$$

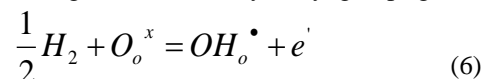
The type of temperature dependence of Ac conductivity indicates that the conduction in the material is a thermally activated process in which the motion of oxygen vacancies gives rise to an activation energy which is considered as the mobile charge carriers.

The Arrhenius plots are estimated from the conductivity data using the Arrhenius equation. In air atmosphere, the Arrhenius plot of the sample measured displayed a linear trend from 200°C to 500°C as shown in the Fig 8. Here, the conductivity depicted a lower value with slightly higher activation energy in air when compared to wet atmosphere as there is no water content present for proton conduction mechanism to take place. The conductivity values of BaCe_{0.65}Zr_{0.2}Y_{0.15}O₃ is found to be of 2.2x10⁻³S/cm and 2.76 x10⁻³S/cm at 500°C in dry air and wet air atmosphere with 3% relative humidity. The conductivity depicted enormous rise with increase in temperature from ~10⁻⁶S/cm at room temperature to ~10⁻⁵S/cm above 300°C. In the present composition as trivalent Y³⁺ replaces Ce⁴⁺, oxygen vacancies are created which in turn trap protons that make defect pairs to aid in the formation of electric dipoles [27].

In ABO₃ perovskite presence of oxygen vacancies result in the formation of protonic defects due to dissociative absorption of water which is represented by Kröger-Vink notation as follows. The formation of hydroxyl ions with oxygen vacancies initiate on the oxygen ion site for the incorporation of water through



The mechanism of proton migration accompanied by series of jumps from one position to another is proposed by Iwahara [6] and further experimented by Kreuer [4]. In the presence of hydrogen, hydrogen possibly reacts with oxide ions in the lattice producing electrons and hydroxyl groups given by the reaction



The mechanism of proton migration accompanied by series of jumps from one position to another is proposed by Iwahara [6] and further experimented by Kreuer [4]. Oxygen vacancies are considered to be the main defects at high temperatures. The activation energy (0.5eV) is determined from the slope of the plot Log σ vs. 1000/T which is lesser than that of the reported value available in literature [15, 29].

Dielectric constant (ϵ'):-

The variation of Dielectric constant with temperature (200°-500°C) and frequency (20Hz to 10⁶Hz) is studied. From the frequency dependent plot Fig 9 it was observed that the value of ϵ' decreases sharply with the increment in the values of frequency. The higher values of dielectric constant at low frequencies can be due to space charge polarization (power frequencies) which occurs due to accumulation of charges at the interfaces in between the electrode and the sample. In low frequency regions the dipoles will get adequate time to orient themselves completely along the field direction when an alternating field is applied on the sample, resulting in larger values of ϵ' of the samples. As the frequency increases further, the dipoles in the samples cannot reorient themselves fast enough in response to the applied electric field but lags behind, resulting in the decrease in ϵ' and reaches a constant value pertaining to higher frequencies applied to the sample up to 10⁶ Hz.

Dielectric permittivity (ϵ''):-

Fig 10 represents the variation of imaginary part of dielectric permittivity (ϵ'') with frequency of the sample at different temperatures and the graph showed a decrease in the (ϵ'') values with ascend in the frequency. The higher values at lower frequency may be due to free motion of charge carriers within the material and as the frequency increases loss increases which reflects a decrease in the value of the dielectric permittivity.

From the plot of dielectric constant versus temperature Fig 11, it was observed that as temperature rises, an increase is observed in the dielectric constant. This can be explained as follows. In space charge polarization, diffusion of ions takes place with a rise in temperature. Additionally, thermal energy may also assist in overcoming the activation barrier for the orientation of polar molecules in the direction of the field which increases the value of ϵ' .

Dielectric loss tangent (tan δ):-

In the presence of alternating field, dipoles align in the direction of field and as time passes by, with the change in the field they rotate again. In the process of alignment energy is lost and a local heat is generated which is the dielectric loss give by loss tangent (tan δ). Fig 12 represents the variation of Tan δ vs. log f at different temperatures. Space charge polarization at grain boundaries (low frequency peak) and dipolar rotations associated to the bulk (high frequency peak) may be responsible for the loss [30, 31]. With increase in the temperature, diffusion of thermally activated protons take place from grains to grain boundaries that result in the decrease in the space charge polarization. The degree to which the dipole is out of phase with the applied field and the losses that develop determine how large the imaginary part of permittivity depends on the material properties and applied frequency. The larger the imaginary part, the more will be the energy dissipated through motion and less is available for propagation through the dipole. Thus imaginary part of relative permittivity (ϵ'') has a direct relation to loss in the system. An overview of the literature available with the present values of conductivity is represented in Table 1.

Table 1:- Conductivity and Activation energies of various compositions.

Composition	Procedure	Conductivity (S/cm)	Activation energy(eV)	Reference
BaZr _{0.2} Ce _{0.65} Y _{0.2} O _{3-δ}	SSR	4.32x10 ⁻³ (500°C)	0.70	[31]
BaZr _{0.2} Ce _{0.65} Y _{0.15} O _{3-δ}	Sol-Gel		0.52(600°C)	[33]
BaZr _{0.1} Ce _{0.7} Y _{0.2} O _{3-δ}	Spray deposition	0.71x10 ⁻³ (400°C)		[34]
BaZr _{0.4} Ce _{0.4} Y _{0.2} O _{3-δ}		2.1x10 ⁻³ (600°C)		[32]
BaCe _{0.85} Y _{0.15} O _{3-δ}		2.5x10 ⁻² (700°C)		[35]
BaCe _{0.85} Y _{0.15} O _{3-δ}	Sol-Gel	7.4x10 ⁻⁴ (400°C)	0.6	[29]
BaCe _{0.35} Zr _{0.5} Y _{0.15} O _{3-δ}	SSR	10 ⁻² (400°C)	0.22	[25]
BaCe _{0.65} Zr _{0.2} Y _{0.15} O _{3-δ}	Sol-Gel	2.2x10 ⁻³ (500°C dry air) 2.76x10 ⁻³ (500°C wet air)	0.53 0.51	This work

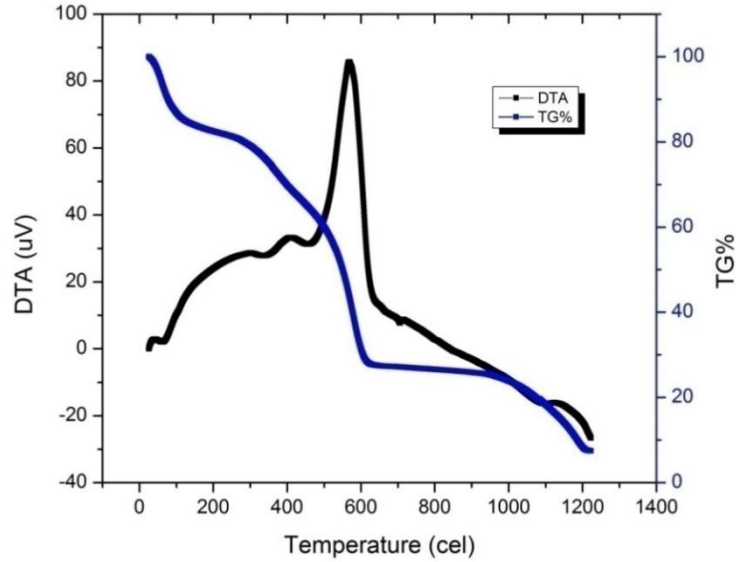


Fig 1:- TG-DTA curves of $BaCe_{0.65}Zr_{0.2}Y_{0.15}O_{3-\delta}$ powder preheated at $250^{\circ}C$ for 24h.

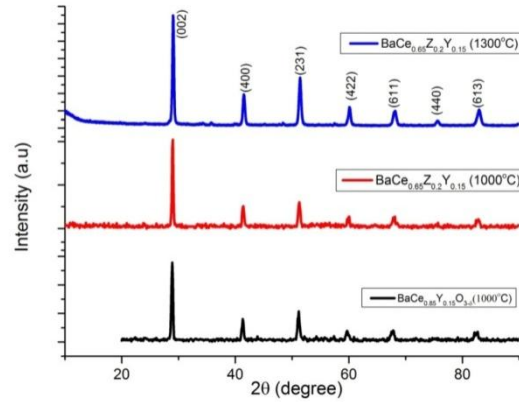


Fig. 2a:- XRD patterns of calcined and sintered $BaCe_{0.65}Zr_{0.2}Y_{0.15}O_{3-\delta}$ oxides .

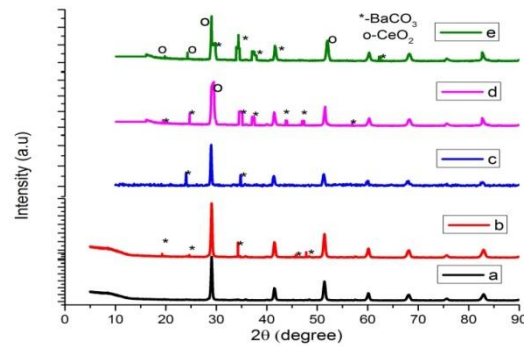


Fig. 2b:- XRD patterns of sintered $BaCe_{0.65}Zr_{0.2}Y_{0.15}O_{3-\delta}$ (a) sintered (b) exposed to H_2O (c) exposed to CO_2 and sintered $BaCe_{0.85}Y_{0.15}O_3$ (d) exposed to H_2O (e) exposed to CO_2 oxides.

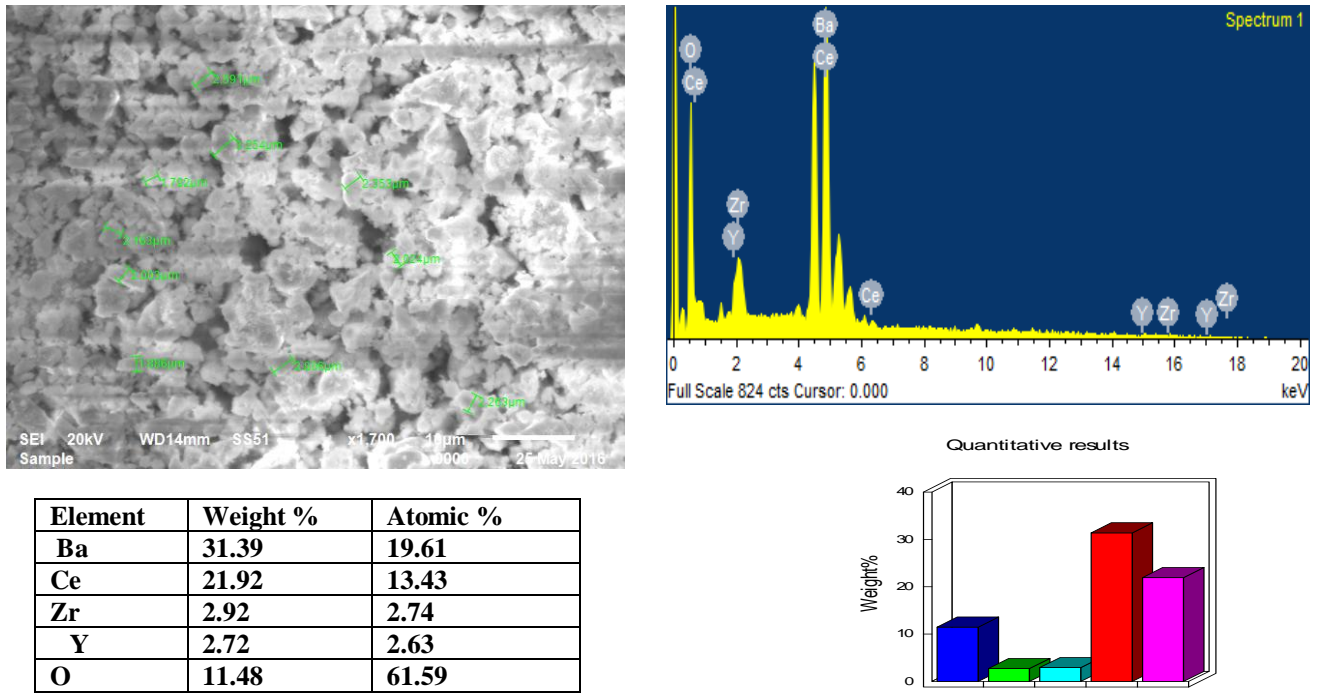


Fig 3:- SEM images and elemental analysis of sintered (1300⁰C/5h) BaCe_{0.65}Zr_{0.2}Y_{0.15}O_{3-δ} oxides.

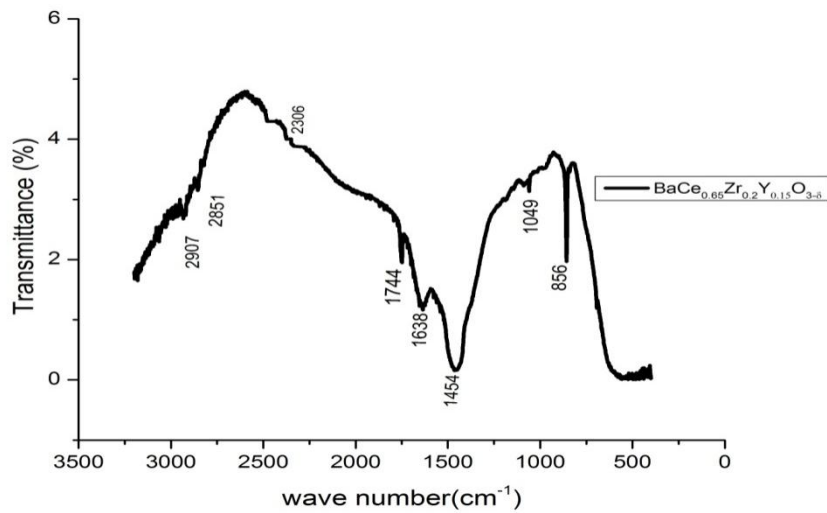


Fig 4:- FTIR spectra of sintered (1300⁰C/5h) BaCe_{0.65}Zr_{0.2}Y_{0.15}O_{3-δ} oxides.

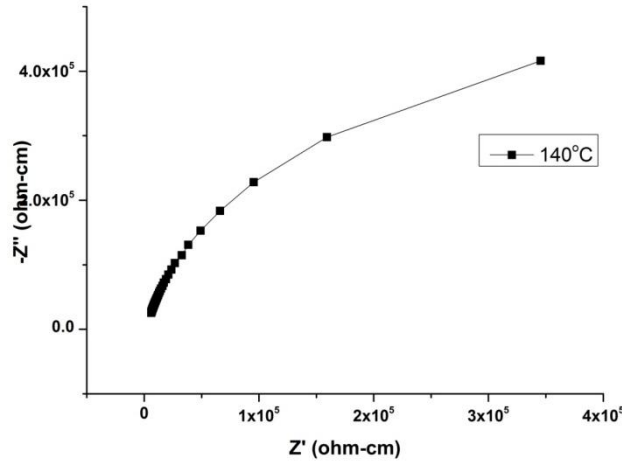


Fig 5:- Nyquist plots of sintered $BaCe_{0.65}Zr_{0.2}Y_{0.15}O_3$ oxide.

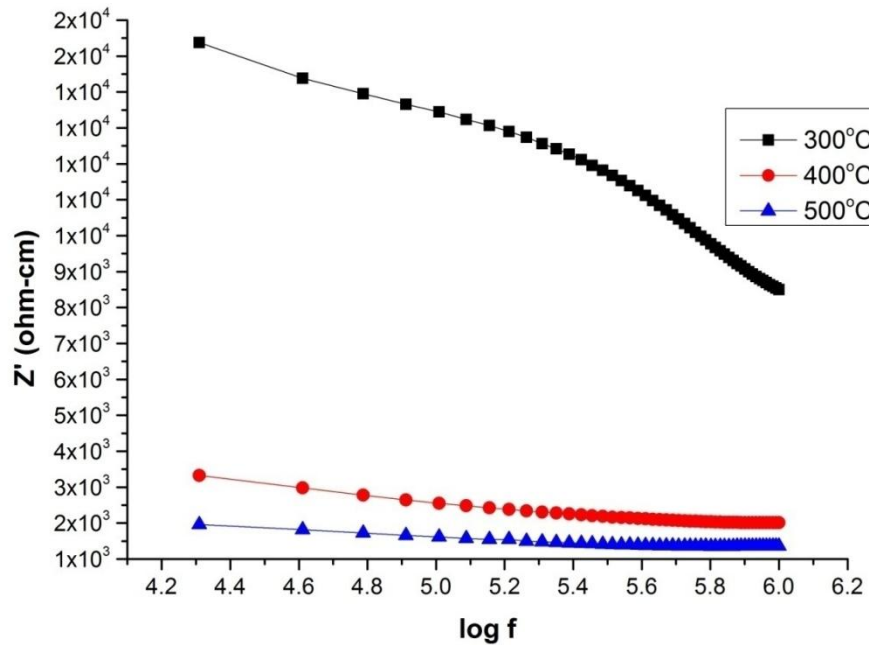


Fig 6:- Variation of Z' with frequency for $BaCe_{0.65}Zr_{0.2}Y_{0.15}O_{3-\delta}$ oxide.

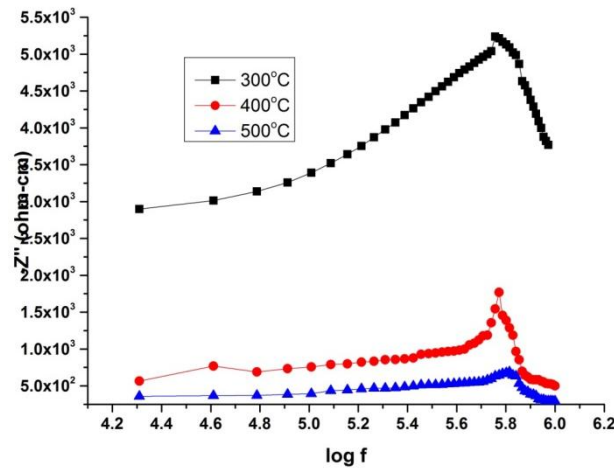


Fig 7:- Variation of Z'' with frequency for $BaCe_{0.65}Zr_{0.2}Y_{0.15}O_{3-\delta}$ oxide.

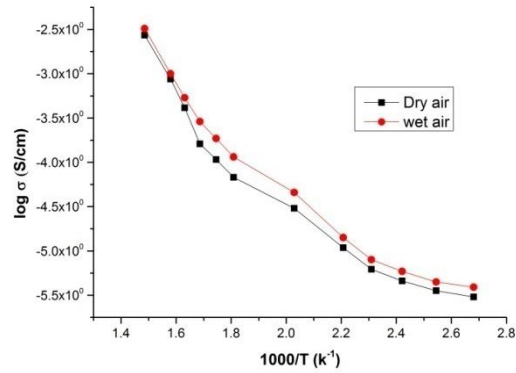


Fig 8:- Arrhenius plot of conductivity in dry air and wet air with 3% relative humidity for samples sintered ($1300^{\circ}C/5h$) $BaCe_{0.65}Zr_{0.2}Y_{0.15}O_{3-\delta}$ oxides.

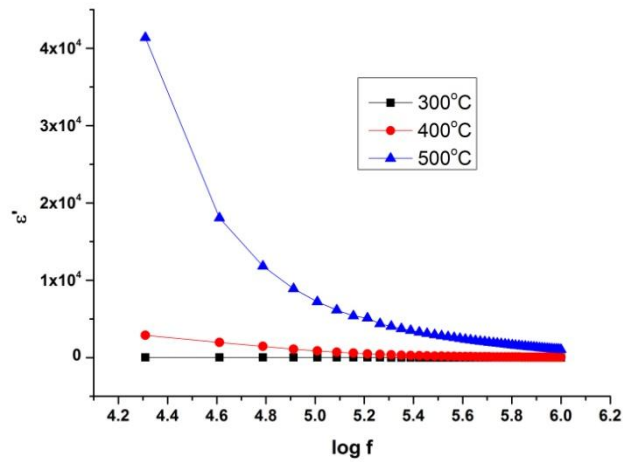


Fig 9:- Variation of dielectric constant with frequency of $BaCe_{0.65}Zr_{0.2}Y_{0.15}O_{3-\delta}$ oxides.

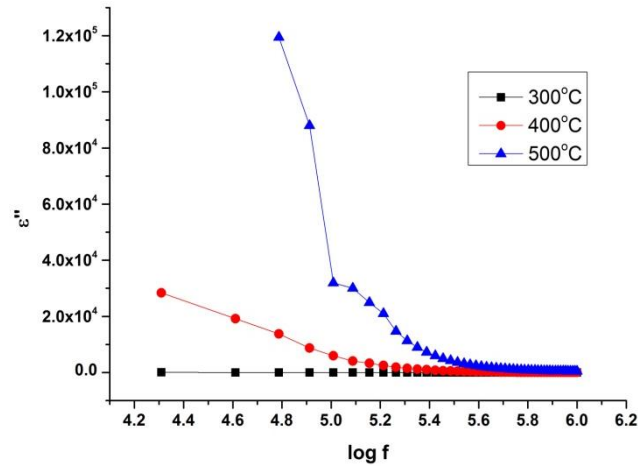


Fig 10:- Variation of imaginary part of dielectric permittivity (ϵ'') vs. frequency of $BaCe_{0.65}Zr_{0.2}Y_{0.15}O_{3-\delta}$ oxides.

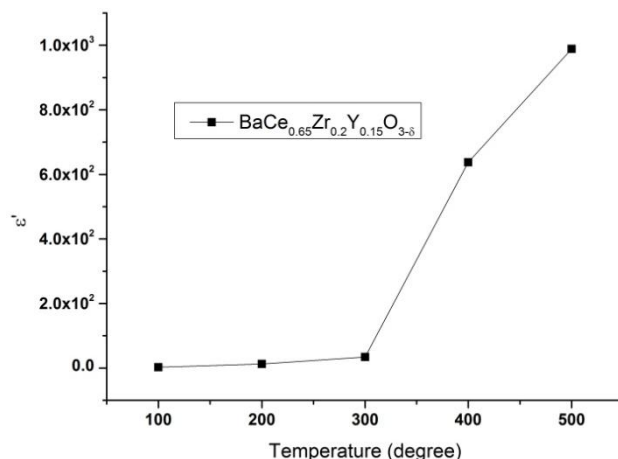


Fig 11:- Variation of dielectric constant with temperature of $\text{BaCe}_{0.65}\text{Zr}_{0.2}\text{Y}_{0.15}\text{O}_{3-\delta}$ oxides.

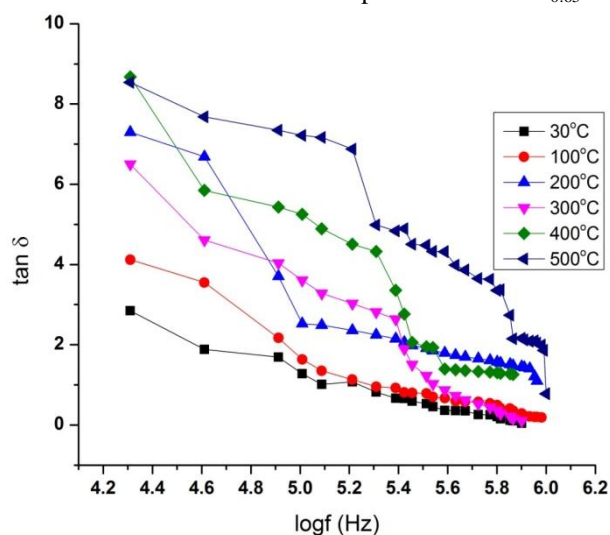


Fig 12:- Variation of $\tan \delta$ with temperature at different frequencies of $\text{BaCe}_{0.65}\text{Zr}_{0.2}\text{Y}_{0.15}\text{O}_{3-\delta}$ oxides.

Conclusion:-

$\text{BaCe}_{0.65}\text{Zr}_{0.2}\text{Y}_{0.15}\text{O}_3$ has been successfully synthesized using the citrate-EDTA complexing sol-gel process at low temperature as low as $T=1000^\circ\text{C}$. The sample showed single phase orthorhombic structure with pmna space group and is consistent with the standard JCPDF data. The crystallite size of the ceramic powders is calculated from Scherrer equation and is found to be 26.45nm and the diffraction peaks shifted to higher angles. Microstructure of the sintered powder revealed that the average grain size is in the range of 2-3 μm . EDX analysis confirmed the elemental composition to be close to the precursor. Dense ceramic materials were obtained at 1300°C and the relative density is 89% of the theoretical density. FTIR measurements reveal the complete of the orthorhombic perovskite structure single phase formation. The ionic conductivities of the pellet are investigated from room temperature to 400°C and is found to be of $2.2 \times 10^{-3}\text{S/cm}$ and $2.76 \times 10^{-3}\text{S/cm}$ at 500°C in dry air and wet air atmosphere with 3% relative humidity. The conductivity increased as temperature increases and the activation energies is 0.5eV. From the results above it is proved that this method of preparation yields good electrolyte which exhibited enhanced conductivity value at low sintering temperature with increased density. Further increase in sintering temperature may increase the density but there is a chance of evaporation of Ba at high temperatures. Further research on using of sintering aid to obtain dense samples without rise in sintering temperature along with trivalent dopant is under process.

Acknowledgements:-

The authors wish to thank the Coordinator DST-Purse programme, Advanced Analytical laboratory, Andhra University for providing XRD, SEM, FTIR and LCR measurements used in this work.

References:-

1. C. Lutgard, D. Jonghe, P. C. Jacobson and S. J. Visco, *Annul. Rev. Mater. Res.* 2003, 33, 169-182.
2. E. Bompar, R. Napoli, B. Wan and G. Orsello, *Int. J. Hydrogen energy.* 2008, 33, 3243-3247.
3. R.O. Fuentes and R. T. Baker, *Int. J. Of Hydrogen Energy.* 2008, 33, 3480-3484.
4. K. D. Kreuer, *Annual .Rev. Mater. Res.* 2003, 33, 333-359.
5. B. Zhuand R. Ljungberg, *Int. J. Hydrogen Energy.* 2008, 33, 3385-3392.
6. H. Iwahara, Y. Asakura, K. Katahirac and M. Tanaka, *Solid Sate Ionics.* 2004,168, 299-310.
7. T. Hibino, A. Hashimto, M. Suzuki and M. Sano, *J Electro Chem. Sco.* 2002,149, 1503-1508.
8. Y. Akimune, K. Matsuo, H. Higashiyam, K. Honda, M. Yamanaka, M. Uchiyama and M. Hatano, *Solid StatIonics.* 2007,178,575-579.
9. Y. Lin, R. Rana, Y. Zheng, Z. Sha,W. Jin, N. Xu and J. Ahn, *J Power Sources.* **180** 2008,180, 15-22.
10. S. Wang, F. Zhao, L. Zhang and F. Chen, *Solid State Ionics.* 2012,213, 29-35.
11. E. Fabbri, A. D'Epifanio, E. D. Bartolomeo, *Fuel Cells.* 2008, 8, 69-76.
12. S. M. Haile, G. Staneff, and K. H. Ryu, *J. Mater Sci.* 2001, 36, 1149.
13. S. Barison, M. Battagliarin, T. Cavallin L. Doubova, M. Fabrizio, C. Mortalo,S. Boldrini, L. Malavasi and R. Gerbasi, *J Mater.Chem.* 2008, 18, 5120-5128.
14. C. Zuo, S. Zha, M. Liu, M. Hatano and M. Uchiyama, *Adv. Mater.* 2006, 18, 3318-3320.
15. F. Deganello, G. Marci, G. Deganello, *J Eur Ceram Soc.* 2009, 29, 439e50.
16. R. R. Chien, C. S. Tu, V. H. Schmidt, S. C. Lee and C. C. Huang, *Solid State Ionics,* 2010,181, 1251-1257.
17. N. Osman, N. A. Ibarahim, M. A. M. Ishak and O. H. Hassan, *Sains Malaysia.* 2014, 43, 1373-1378.
18. L. Malavasi, C. A. J. Fisher and M. S. Islam, *Chem. Soc. Rev.* 2010, 39, 4370-4387.
19. H. Ding and X. Xue, *J Power Sources.* 2010,195, 7038e41.
20. S. U. Dubai, A P. Jamale , C. H. Bhosale, L. D. Jadhav, *Appl. Surf. Sci.* 2015, 325, 871-876.
21. T. Ohzeki, S. Hasegawa, M. Shimizu and T. Hashimoto, *Solid State Ionics.* 2009,180, 1034-1039.
22. Y. Guo, R. Ran, Z. P. Shao, and S. Liu, *Int J Of Hydrogen Energy.* 2011,36, 8480-8460.
23. L. U Jingde, L. Wang, L. Fan and H. Guo, *J Rare Earth* 2008,26, 504-510.
24. Z. Shi, W. Sun, Z. Wang, J. Qiant, and W. Liu, *Appl .Mater. Interfaces.* 2014, 6, 5175-5182.
25. B. A. Kumar, S. Choi, B. K. Kim, J. H. Lee, *Mater. Renew. Sustain Energy.* 2014, 3, 1-9.
26. K. D. Krekuer, *Solid State Ionics.* 1997, 97, 1-15.
27. Y. Yamazaki, R. H. Sanchez, S.M Haile, *J Mater Chem.* 2010,81, 58-66.
28. Agnieszka Lacz, Katarzyna Grzesik and Pawel Pasierb, *J Power Sources.* 2015,279, 28-35.
29. J. Madhuri Sailaja and V. Veeraiah, *Journal of Advances Research in Science and Engineering,* 2016,5 128-138.
30. K. Christian, F. Harald, P. Øystein, I. D. Paul, E. Claude, H. Reidar and N. Truls, *Solid State Ionics.* 2010,181, 268-275.
31. D. K. Lim, C. J. Park, M. B. Choi, C. N. Park and S. J. Song, *Int. J. Hydrogen Energy.* 2010, 35, 10624-10629.
32. Y. M. Gyo, R. Ran and Z. P. Shao, *Int J Hydrogen Energy,* 2010,35, 5611-20.
33. L. Doubova, S. Barison, S. Boldrini, C. Pagura, *J.Appl Electro Chem.* 2009,39, 2129-2141.
34. L. Yang, S. Wang, X. Lou and M. Liu, *International Journal of Hydrogen Energy.* 2011, 36, 2266-2270.
35. G. Raikova, M Krapchanska, I. Genov, G. Caboche, L. Combemale and A. Thorel, *Bulgarian Chemical Communications.* 2012,44,389-394.